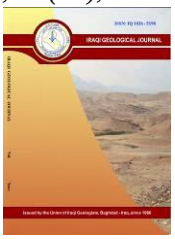
Iraqi Geological Journal

Journal homepage: https://www.igj-iraq.org



Geochemistry of Lava Gamalama Volcano, Indonesia: Implications for Magma Genesis and Tectonic Setting

Yanny Yanny[1,3*], Adi Maulana[2], Musri Mawaleda[2], and Ulva Ria Irfan[2]

1 Earth and Environment Technology Study Program, Faculty of Engineering, Hasanuddin University, Makassar, Indonesia
2 Department of Geology Engineering, Faculty of Engineering, Hasanuddin University, Makassar, Indonesia
3 Mining Engineering Program Study, Faculty of Engineering, Muhammadiyah University of North Maluku, Ternate, Indonesia
* Correspondence: yanny23@ummu.ac.id, adi-maulana@unhas.ac.id

Received:
18 April 2025
Accepted:
25 October 2025
Published:
31 January 2026

Abstract

Gamalama Volcano (Ternate Islands, North Maluku, Indonesia) is an active arc stratovolcano. To investigate magma genesis and the tectonic setting of recent Gamalama lavas, we combined petrographic observations with whole-rock major- and trace-element analyses. Five fresh samples, representing the Young Gamalama phase, were examined petrographically and analysed for major elements by XRF and for trace and rare-earth elements by ICP-OES/ICP-MS. The lavas are basaltic–andesitic (SiO_2 = 52.1–55.7 wt.%) and plot in the calc-alkaline, medium-K field. Petrography shows abundant plagioclase (andesine–labradorite), clinopyroxene, and Fe–Ti oxides embedded in the groundmass; local plagioclase chloritization records limited secondary alteration. Major-element variation diagrams (Harker, AFM) indicate early clinopyroxene and Fe–Ti oxide fractionation followed by late plagioclase crystallization, with subordinate evidence for periodic magma mixing. Trace-element and rare earth element systematics display large-ion lithophile elements and light enrichment and pronounced negative Nb–Ta anomalies, consistent with slab-influenced arc magmatism. The Nb–Ta depletion may reflect rutile sequestration in slab residues and/or transfer by saline slab-derived fluids; both mechanisms are considered viable. Tectonic discrimination diagrams (La/Yb vs Th/Nb; La/Yb vs Nb/La) place the samples in the volcanic-arc field, consistent with eastward subduction of the Molucca Sea Plate beneath Halmahera. These findings provide new constraints on petrogenesis of the Young Gamalama lavas and underscores the necessity of future multidisciplinary studies to unravel the volcano's longer-term magmatic evolution.

Keywords: Basaltic–andesitic; Calc-alkaline; Fractional crystallization; Volcanic arc

1. Introduction

1.1 Background

Gamalama volcano forms a dominant topographic feature of Ternate Island in Indonesia's northern Moluccas. As one of the country's most active stratovolcanoes, it reaches an elevation of 1,714 m and has a documented eruptive history stretching back to the 16th century (Global Volcanism Program [GVP], 2025). Most activity is focused at a steep summit crater, approximately 150 x 180 m wide and 100 m deep, which hosts persistent fumaroles emitting gases such as CO_2, SO_2, and H_2S (Bani et al., 2021; Kunrat et al., 2020; Suhermat et al., 2024). Notably, significant eruptions have also occurred on

its flanks, including a 1907 event that produced lava flows extending to Kulaba Beach, forming the Batu Angus lava field (Awal et al., 2020).

This Holocene-aged volcano is primarily constructed of basaltic–andesitic lavas, andesitic breccias, and pyroclastic tuffs (Ningrum et al., 2019). Its lower slopes feature three prominent maars-Tolire Jaha, Tolire Kecil (Small Tolire) Maar, and Ngade Maar, which constitute key geomorphological landmarks (Hidayat et al., 2020; Fig.1). Over the past decade, Gamalama has erupted frequently, with an average recurrence interval of one to two years (GVP, 2025). These recent eruptions are predominantly phreatic or phreatomagmatic, controlled by summit fractures linked to regional tectonic structures (Kunrat et al., 2020). A well-documented example is the September 2015 eruption, which generated an ash plume rising ~2 km high above the summit crater (GVP, 2025).

Previous research on Gamalama has provided valuable insights into its geochemical and structural characteristics. Whole-rock geochemistry indicates its lavas are calc-alkaline, ranging from basaltic–andesitic to andesite, consistent with a subduction-related magmatic origin (Ansori et al., 2024). Spectroscopic studies have identified silica functional groups, including siloxane (≡Si-O-Si≡), siloxyl (≡Si-O-), and silanol (≡Si-OH), in volcanic materials (Yanny et al., 2020). Fumarolic gases, with temperatures of 425–480 °C, indicate a hybrid magmatic-hydrothermal source (Kunrat et al., 2020). A significant morphological change occurred post-2002, with the summit crater evolving from a simple circular structure to a fractured system, diverting activity to peripheral zones. This structural evolution is supported by geochemical evidence, notably a high CO_2/S_T ratio of 20.9, suggesting shallow hydrothermal activity overprinting magmatic degassing (Bani et al., 2021).

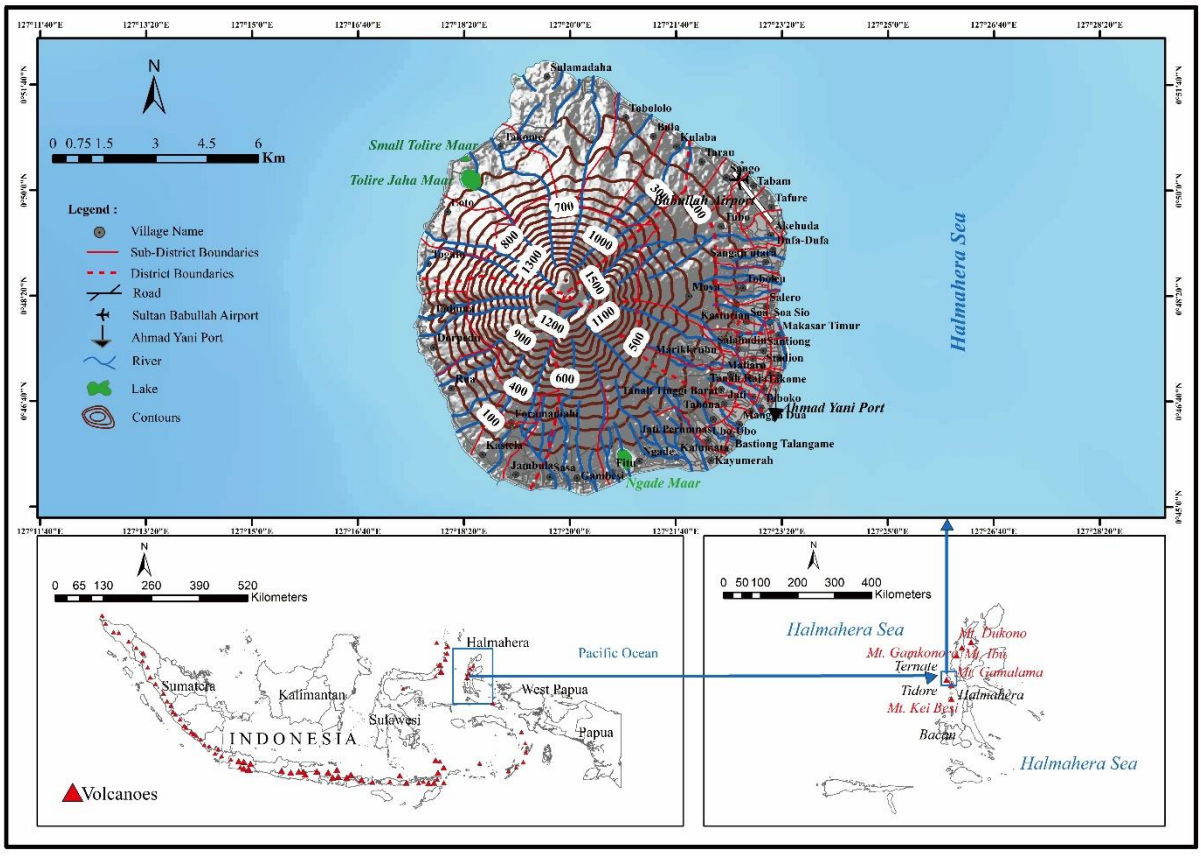


Fig.1. The three main maars (Tolire Jaha Maar, Small Tolire Maar, and Ngade Maar) of Gamalama volcano, surrounded by residential areas and public infrastructure, including ports and an airport (Hidayat et al., 2020)

However, the magmatic evolution of Gamalama remains poorly constrained, particularly regarding the application of rare earth element (REE) geochemistry to elucidate differentiation processes and

mantle source characteristics. Our study addresses this gap by integrating detailed petrographic analysis with comprehensive major oxide, trace element, and REE data. Petrographic characterizes mineral assemblages and textures, while geochemical data interrogate magmatic processes and source enrichment. Together, these methods provide new constraints on the petrogenesis of the Young Gamalama lavas and their implications for the tectonic framework of the Halmahera arc.

1.2. Geological Settings

The North Maluku region in eastern Indonesia occupies one of the most structurally complex convergent plate boundaries on Earth, situated at the triple junction of the Eurasian, Indo-Australian, and Philippine Sea plates (Wang et al., 2023). Tectonic convergence in this area is primarily accommodated within the Molucca Sea Collision Zone, which hosts a rare double-sided subduction system. In this setting, the oceanic Molucca Sea Plate is being consumed simultaneously along its western and eastern margins: the western limb subducts beneath the Sangihe Arc, while the eastern limb descends beneath the Halmahera Arc (Widiwijayanti et al., 2004; Olfindo et al., 2019) (Fig. 2).

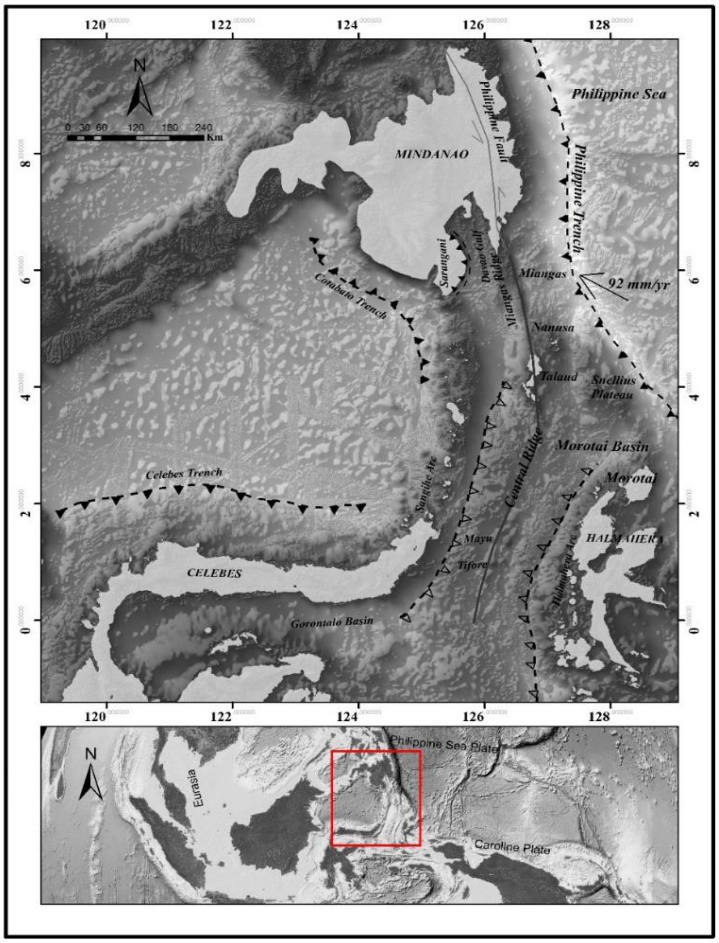


Fig.2. Collision of the Halmahera and Sangihe oceanic arcs in the Molucca Sea (modified from Widiwijayanti et al., 2004)

The Sangihe–Halmahera double arc records a Neogene tectonic reversal in the Molucca Sea region, driven by the rotation and northward motion of the Philippine Sea Plate. Subduction initiated beneath the Sangihe Arc at ~20 Ma but ceased by ~10 Ma, after which it switched to the Halmahera side, triggering volcanic activity there by ~8 Ma (Hall and Spakman, 2015; Hinschberger et al., 2005). This tectonic switch produced a pronounced asymmetry in the modern subduction system. Seismological and seismic tomography data show that the Halmahera slab dips eastward and remains active only to

intermediate depths (~35–400) km, whereas the Sangihe slab penetrates the lower mantle, with seismicity extending to ~660 km (Hall and Spakman, 2015; Suhardja et al., 2024). The ongoing northward motion of the Philippine Sea Plate continues to shape this complex collision zone, sustaining dynamic stress interactions between the two arcs.

Gamalama volcano exemplifies the magmatic consequences of the Late Neogene tectonic reversal in the Molucca Sea region. Located on Ternate Island, west of the main Halmahera volcanic front, Gamalama is situated within the active Halmahera Arc and derives its magmatism from ongoing subduction of the Molucca Sea Plate. The samples analysed in this study, representing the Young Gamalama eruptive phase, thus offer a geochemical record of mantle–slab interactions in a subduction system that has been active since ~8 Ma (Hall and Spakman, 2015).

2. Materials and Methods

Gamalama volcano has a complex stratigraphy, divided into three main eruptive phases: Old Gamalama, Mature Gamalama, and Young Gamalama (Bronto et al., 1982). We collected a total of fifteen lava samples from outcrops in the northeastern sector of the volcano (around the Batu Angus site; see Fig.3). These lavas belong to the Young Gamalama Formation (Holocene) and were selected based on their relatively fresh condition (minimal weathering) to represent recent eruptive products. From this collection, five samples were chosen for detailed geochemical analysis. The selection strategy was designed to ensure the samples encompass a variety and spatial distributions and distinct lava flows, thereby capturing compositional variability within this eruptive phase, while avoiding repetition from very similar flows.

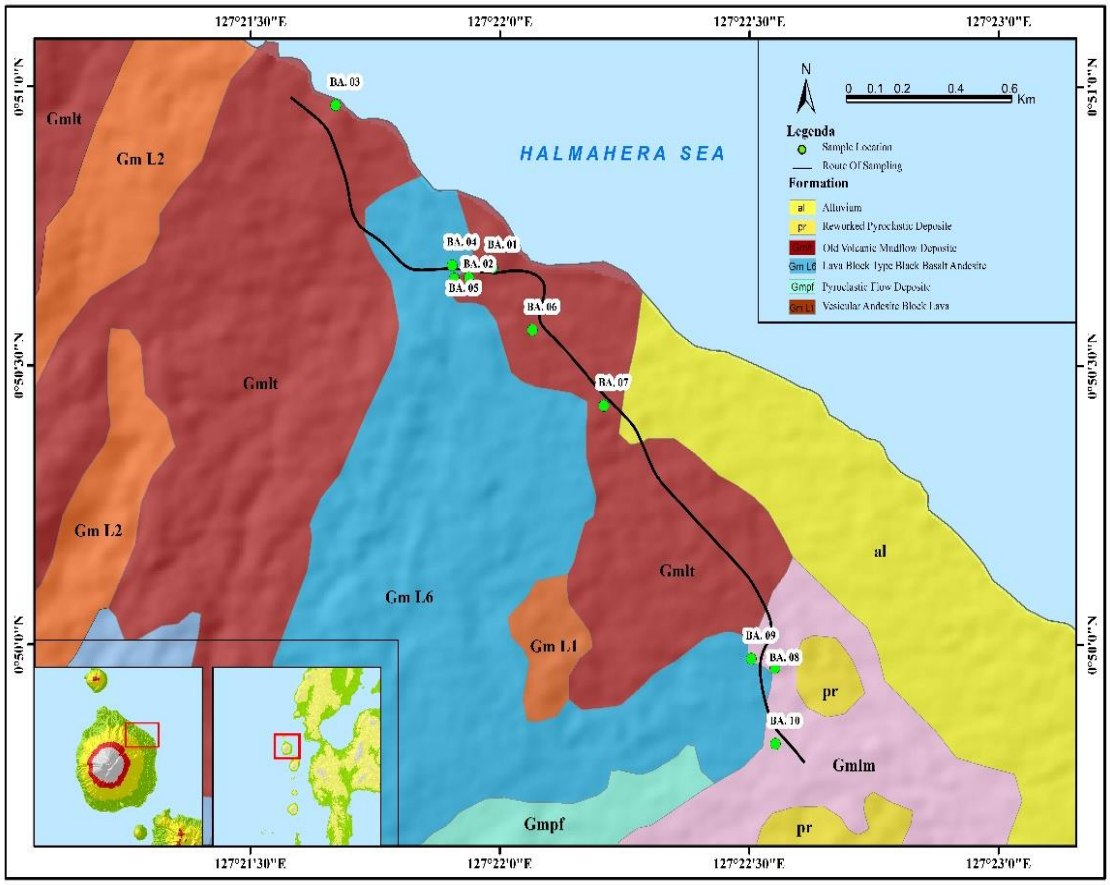


Fig.3. Geological map of the study area showing the sampling locations (Young Gamalama phase) (after Bronto et al., 1982)

To minimize contamination and alteration, we attempted to collect fresh samples. During sampling, duplicate specimens and field descriptions were recorded for cross-verification. The samples were labeled (e.g., BA.01, BA.02, and so on) and documented.

Subsequently, the samples were prepared for petrographic and geochemical analyses, conducted in the Rock Preparation Laboratory, Geological Engineering, Hasanuddin University. Petrographic observations were conducted at the Optical Mineralogy Laboratory, Geological Engineering, Hasanuddin University, using a trinocular polarizing microscope (Nikon LV100POL with a DS-Ri1 camera and NIS-Elements software). Mineral phases were identified and described in parallel and cross-polarized light. Texture (e.g., grain size, crystal form, zoning), phenocryst composition (plagioclase, pyroxene, and opaque), and the nature of any secondary alteration phases (e.g., chlorite) were also analyzed.

The prepared samples, in 200-mesh powder form, were then sent to the Intertek Analytical Laboratory in Jakarta for geochemical analysis. Major–element oxides were measured by wavelength-dispersive X-ray fluorescence (XRF) after lithium metaborate fusion. Trace and rare earth elements (REE) were determined using inductively coupled plasma methods: selected major and minor elements by Inductively Coupled Plasma-Optical Emission Spectroscopy (ICP-OES; Scheme 4A/OE), and trace elements including REE by Inductively Coupled Plasma-Mass Spectrometry (ICP-MS; Schemes 4A/MS and 4A/MS11). Samples were digested using a four-acid protocol in closed Teflon tubes, following Intertek standard procedures. Total iron was measured as Fe_2O_3 by XRF, but is expressed as FeO_t in variation diagrams for consistency with standard geochemical classification schemes.

Typical detection limits for XRF are on the order of 0.01–0.002 wt.% for major oxides. For solution-based methods, ICP-OES generally provides detection limits in the range of 1–100 ppm for trace elements, while high-resolution ICP-MS can achieve much lower detection limits, typically 0.05–0.1 ppm for most trace and rare earth elements. Results are reported as weight percentages of oxides (major elements) and ppm (trace elements, including REEs) in Table 1. The data are used to construct variation diagrams (e.g., Harker plots of oxides vs. SiO_2) and tectonic discrimination plots (e.g., SiO_2–K_2O, AFM, La–Yb vs. Th–Nb) using standard references. These plots aid in the interpretation of magma affinities, differentiation processes, source characteristics, and tectonic settings.

3. Results

3.1. Petrology

In the field, fresh lava generally exhibits colors ranging from dark gray to light gray, while weathered surfaces appear brownish-gray. Textures vary from massive to vesicular. Common surface features include well-developed vertical joint sets interpreted as probable columnar jointing-togather with subordinate subhorizontal cooling joints and abundant clinker fragments (Fig.4). These basaltic–andesitic flows are widely exposed in roadside cuts, slopes, coastal outcrops, and residential areas, and occur in association with volcaniclastic deposits and laharic breccia composed of angular to subangular clasts within a clay-rich matrix. This relationship is consistent with effusive emplacement followed by syn-or post-eruptive remobilization of pyroclastic material, influencing the distribution and reworking of volcanic deposits during the Young Gamalama phase. The identification of columnar jointing is preliminary, being based mainly on lateral exposures; confirmation from fresh transverse sections or detached blocks is recommended.

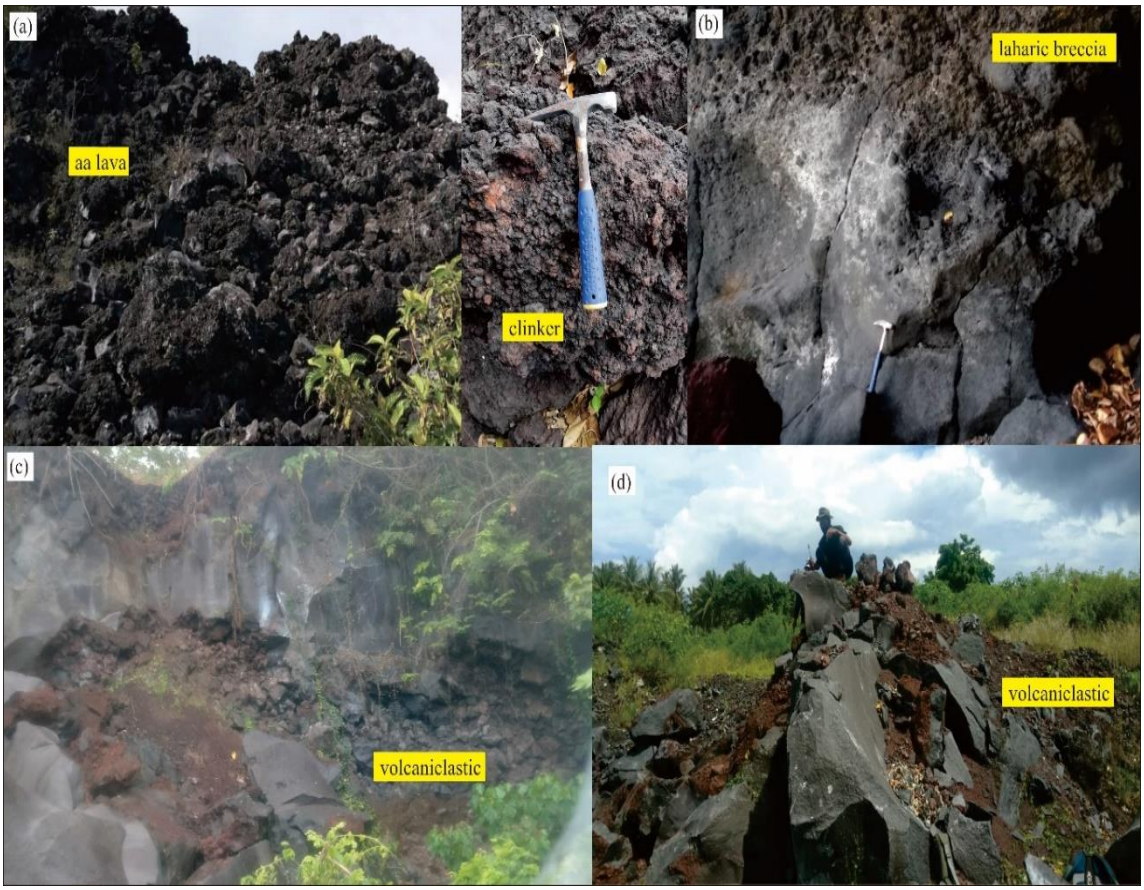


Fig.4. Representative outcrops of Young Gamalama lavas showing variations from: a) Vesicular clinker-rich flows BA.01, BA.02, BA.04, and BA.05; b) Vertical-jointed lava overlain by laharic breccia at station BA.03; c) Massive lava at station BA.07; d) Lava associated with volcaniclastic deposits at station BA.10

Petrographic observations on fifteen thin sections show that the lavas are fine-grained with hypocrystalline, porphyroaphanitic textures (Fig.5). Plagioclase is the dominant phenocryst phase (about 35–45%), occurring as subhedral tabular crystals (0.1–1.3 mm) with polysynthetic and Carlsbad-albite twinning. Extinction angles (about 15–17°) indicate compositions ranging from labradorite to andesine. Plagioclase exhibits various textures, including glomeroporphyritic aggregates with pyroxene and opaques, as well as oscillatory zoning and sieve textures in some samples; corrosion features are also observed on crystal margins (Fig. 6). These textures suggest open-system processes such as magma mixing, decompression, or reheating prior to eruption. Clinopyroxene (about 4–17%) occurs as subhedral short prisms (0.2–1.0 mm) with pale gray coloration in PPL, high interference colors in XPL, and inclined extinction angles of about 20–25°, consistent with augite (Nesse, 1991; Deer et al., 2013). Opaque minerals (about 4–5%), mainly iron oxides, occur as anhedral grains smaller than 0.2 mm. The groundmass is composed of plagioclase microlites (about 20–25%), fine-grained pyroxene, and abundant volcanic glass (about 27–35%); the high glass content reflects rapid cooling and quenching of the melt (Gill, 2010; Scarani et al., 2022), which inhibited extensive crystallization. Chlorite (~3%) occurs locally as a secondary mineral replacing plagioclase microlites (Fig.5), indicating post-emplacement hydrothermal alteration.

Based on modal estimates (n = 15) and classification using QAPF criteria (Streckeisen, 1979), the rocks are identified as basaltic–andesitic. This petrographic classification is consistent with whole-rock geochemical data, providing a foundation for the interpretations discussed in the following sections.

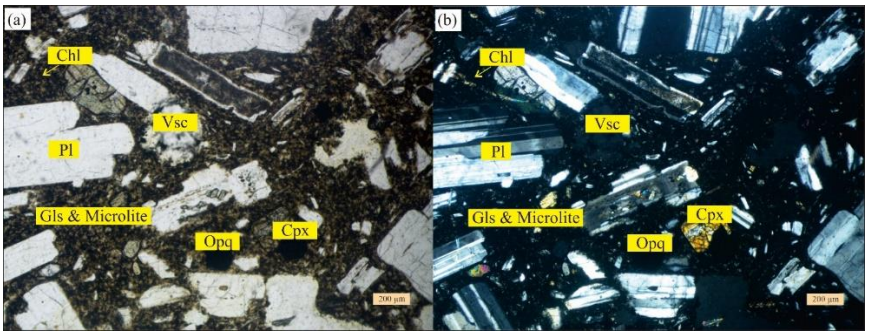


Fig. 5. a) Photomicrograph of basaltic–andesitic BA.02 in the appearance of parallel Nicol bars 200 µm; b) Appearance in cross-nicol magnification 200 µm, consisting of plagioclase phenocrysts (Pl), clinopyroxene (Cpx), and opaque minerals (Opq) in the glass and crystal groundmass, and there are secondary minerals in the form of chlorite (Chl)

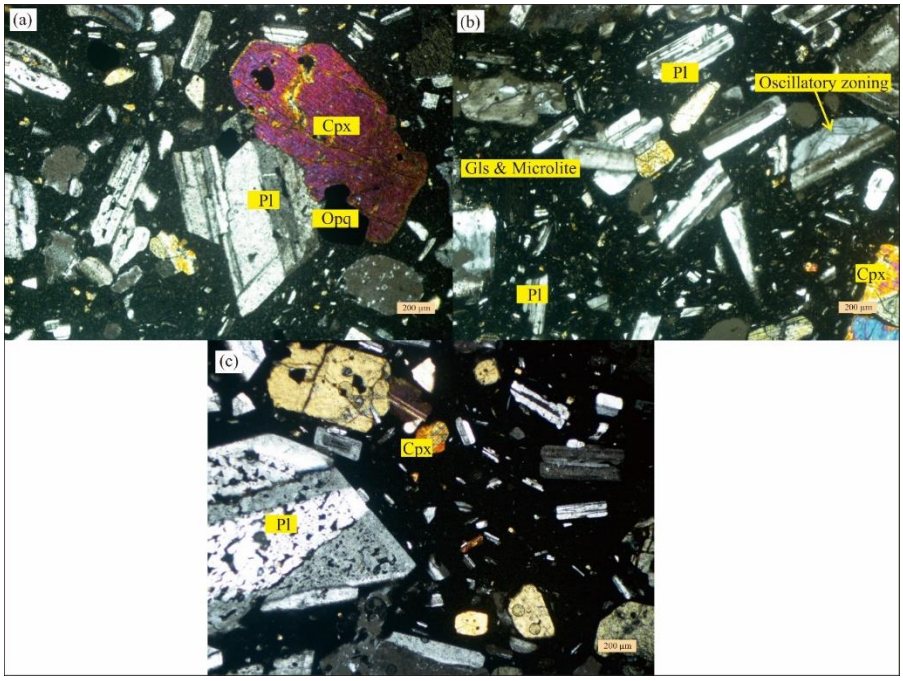


Fig.6. Photomicrographs of basaltic andesite under crossed polars (XPL), scale bar = 200 µm: a) BA.10-FA showing a glomeroporphyritic texture of plagioclase, pyroxene, and opaque minerals; b) BA.07 showing plagioclase phenocrysts (Pl) with oscillatory zoning; c) BA.10-MC showing corroded plagioclase phenocrysts (Pl) with sieve texture

3.2. Major Elements

To complement petrographic observations, whole-rock geochemical analyses were carried out to constrain the composition and magmatic evolution of the Gamalama lavas. Major-element data, obtained by X-ray fluorescence (XRF) spectrometry, are presented in Table 1. The lavas show a restricted silica range (52.13–55.69 wt.% SiO_2), consistent with a basaltic andesite composition. Key features include relatively high alumina (19.47–20.72 wt.% Al_2O_3) and moderate variations in CaO (8.43–8.99 wt.%) and total iron (reported as FeO_t: 5.97–8.74 wt.%). Other oxides show the following ranges: Na_2O (3.32–3.73 wt.%), K_2O (0.93–1.45 wt.%), TiO_2 (0.58–0.83 wt.%), MnO (0.11–0.16 wt.%), MgO (2.23–3.98 wt.%), and P_2O_5 (0.17–0.30 wt.%). The consistently low loss on ignition (LOI) values (<0.36 wt.%) confirm that the samples are fresh and only minimally altered, ensuring the reliability of the major element data for petrogenetic interpretation.

Table 1. Major elements (wt.%) and trace elements (ppm) compared with andesite from South Halmahera (BA.X; Ipranta and Irzon, 2019)

	BA.03	**BA.06**	**BA.09**	**BA.10**	**BA.10ME**	**BA.X**
Major oxide (wt.%)						
SiO_2	52.13	55.42	55.69	55.53	55.59	n.d.
Al_2O_3	19.47	19.69	19.70	20.72	20.28	n.d.
Fe_2O_3	9.71	7.37	7.46	6.97	6.64	n.d.
FeO_t[1]	8.74	6.63	6.71	6.27	5.97	n.d.
MnO	0.16	0.11	0.12	0.11	0.12	n.d.
MgO	3.98	2.28	2.67	2.28	2.23	n.d.
CaO	8.99	8.43	8.52	8.86	8.58	n.d.
Na_2O	3.32	3.67	3.55	3.70	3.73	n.d.
K_2O	0.93	1.45	1.39	1.28	1.38	n.d.
TiO_2	0.83	0.65	0.66	0.60	0.58	n.d.
P_2O_5	0.18	0.31	0.19	0.18	0.19	n.d.
LOI	0.36	0.10	<0.01	<0.01	<0.01	n.d.
Total	100	99.50	99.80	100	99.30	n.d.
Trace Elements (ppm)						
Ba	205	290	280	254	315	250.82
Sr	413	429	422	438	458	381.34
Y	20.80	22.40	21.90	19.40	22.60	28.32
Zr	85.20	113	111	98.30	119	n.d.
Rb	19.90	34	31.80	27.30	31	n.d.
Nb	2.10	2.60	2.60	2.30	2.70	3.11
Ta	0.13	0.17	0.16	0.16	0.18	0.33
Pb	8	11	10	9	11	n.d.
Th	5.16	6.92	6.70	5.33	6.42	n.d.
U	0.66	1.11	1.10	0.92	1.06	n.d.
Rare Earth Elements (ppm)						
La	10.90	14.30	14	13.10	14.30	10.30
Ce	31	37.80	37.30	33.20	35.40	24.64
Pr	3.40	4.26	4.19	3.21	4.18	3.66
Nd	15.40	18.30	18.10	15.20	17.40	16.11
Sm	3.70	3.90	3.70	3.60	3.90	4.30
Eu	1.20	1.30	1.30	1.10	1.30	0.95
Gd	3.80	4.40	4.30	3.70	4.30	3.54
Tb	0.58	0.66	0.66	0.54	0.64	0.69
Dy	4.00	4.40	4.30	3.60	3.90	4.76
Ho	0.80	0.80	0.80	0.70	0.80	1.05
Er	2.40	2.30	2.50	2.10	2.40	2.89
Tm	0.30	0.40	0.40	0.30	0.30	0.43
Yb	2.30	2.50	2.50	2.20	2.40	2.83
Lu	0.37	0.38	0.38	0.33	0.38	0.43
Eu/Eu*	0.31	0.33	0.33	0.28	0.33	n.d.
La/Sm	2.95	3.67	3.78	3.64	3.67	n.d.
Gd/Lu	10.27	11.89	11.32	11.21	11.32	n.d.
LREE	69.40	84.26	82.89	73.11	80.78	63.50
HREE	10.75	11.43	11.54	9.87	10.72	13.08
ΣREE	80.15	95.69	94.43	82.98	91.50	76.58

Note: [1]Total iron as FeO ($FeO_t = Fe_2O_3 \times 0.8998$) for consistency with variation diagrams and petrogenetic discussion (see Methods). LOI = loss on ignition; n.d. = no data available.

Classification using the Total Alkali-Silica (TAS) diagram (Le Bas et al., 1986; Middlemost, 1994; Fig.7) shows that all samples plot within the basaltic–andesitic field of the subalkaline series. With total alkalis ($Na_2O + K_2O$) ranging from 4.25–5.12 wt.%, the lavas are classified as medium-K calc-alkaline (Sheth et al., 2002), which is typical of magmas generated in subduction-related tectonic settings.

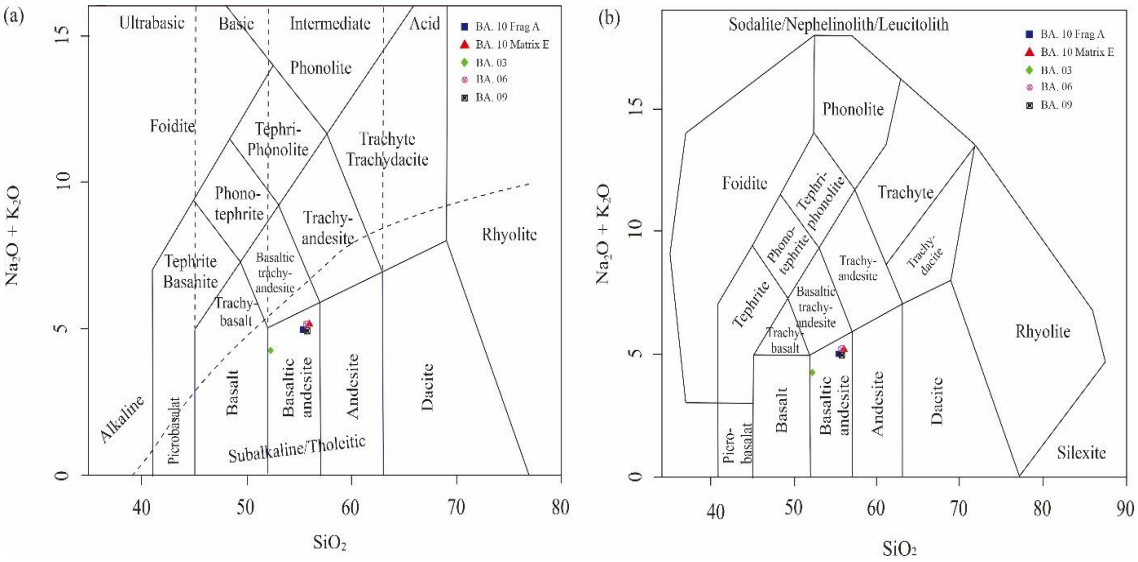


Fig.7. Geochemical classification of Gamalama volcanic rocks based on whole-rock major-element data (wt.%; XRF; Table 1): a) Total Alkali-Silica (TAS) diagram after Le Bas et al. (1986); b) Modified TAS diagram after Middlemost (1994). All samples (n = 5) plot within the subalkaline basalt–andesite field, consistent with a medium-K calc-alkaline affinity characteristic of arc-related magmatism.

Harker variation diagrams (Fig. 8) illustrate systematic oxide-silica relationships. K_2O, Na_2O, and P_2O_5 display positive correlations with increasing SiO_2, whereas TiO_2, FeO_t, MgO, and CaO decrease. The negative CaO–SiO_2 trend is consistent with early clinopyroxene fractionation (Chin et al., 2018), while the positive Al_2O_3–SiO_2 correlation suggests that plagioclase fractionation became significant during later stages. This interpretation implies that the abundant plagioclase phenocrysts observed petrographically crystallized predominantly at a late stage, after substantial Ca had already been removed by clinopyroxene fractionation.

The declining MgO and FeO_t contents with increasing SiO_2 further reflect progressive removal of mafic minerals. Samples with <3.1 wt.% MgO particularly emphasize the role of clinopyroxene fractionation, consistent with observations in other arc settings (Rezaei-Kahkhaei et al., 2011; Molnár et al., 2023). The decrease in TiO_2 with SiO_2 supports early crystallization of Fe–Ti oxides. In Fig.9, weakly positive P_2O_5–SiO_2 trend (R = 0.22) suggests limited apatite crystallization during early differentiation, allowing P to remain relatively enriched in the residual melt (Rezaei–Kahkhaei et al., 2011; Tornos et al., 2024).

Although several oxide–SiO_2 trends are clear, many plots exhibit scatter and relatively low correlation coefficients (see R values annotated on Fig. 9). This scatter, together with petrographic indicators such as sieve textures and oscillatory zoning in plagioclase, is consistent with periodic magma mixing superimposed on fractional crystallization (Korkmaz and Kurt, 2021; Guo and Chen, 2025). The contrasting behavior of CaO (decreasing) and Na_2O (increasing) with SiO_2 is also consistent with compositional zoning in plagioclase (Nurahmah et al., 2024). Collectively, the geochemical and petrographic evidence indicates that the Young Gamalama lavas evolved primarily through fractional crystallization, periodically modified by magma mixing, within an island–arc tectonic setting (Zhao et al., 2021)

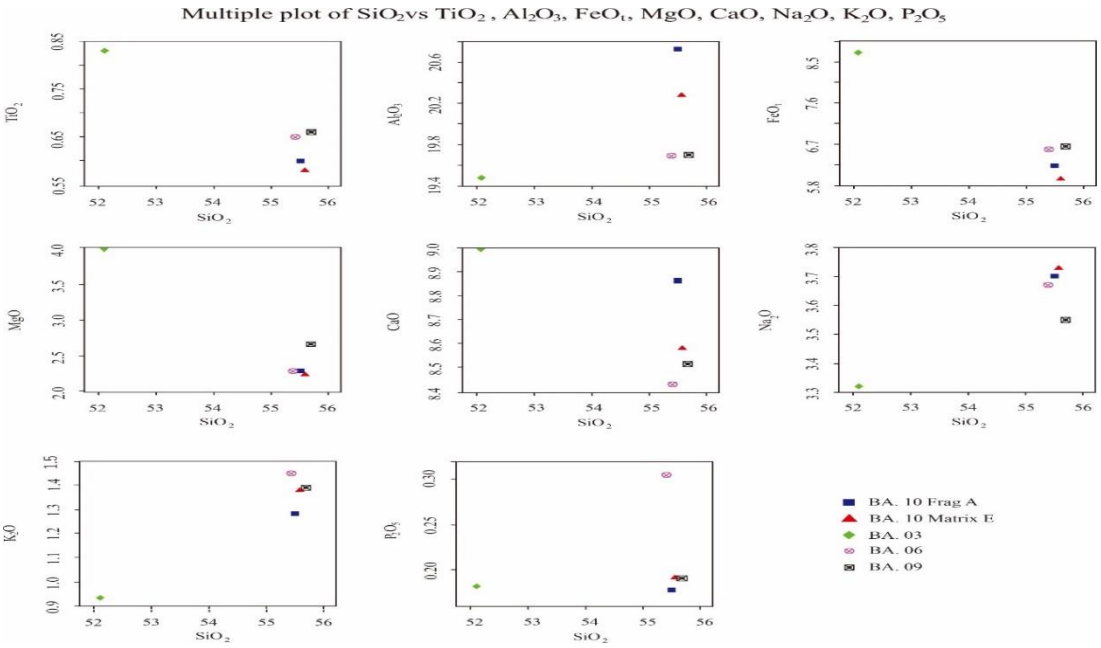


Fig.8. Harker variation diagrams (after Harker, 1909) showing major oxide concentrations versus SiO_2 content for Gamalama volcanic rocks. Data from whole-rock XRF analysis (wt.%; Table 1).

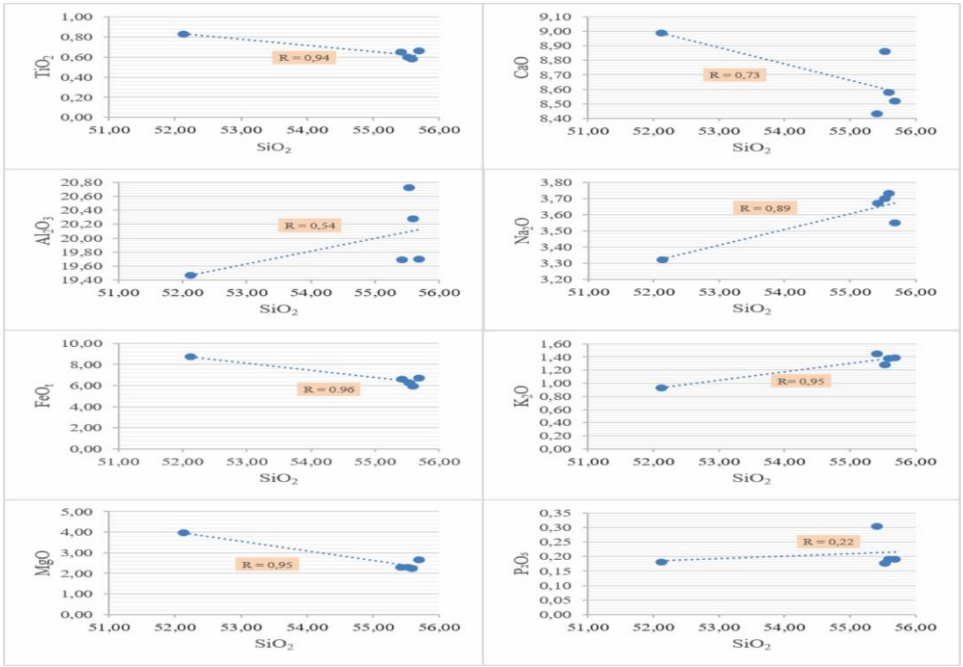


Fig.9. Correlations between SiO_2 and major oxides (wt.%) for Gamalama volcanic rocks, with correlation coefficients (R). Whole-rock major-element data (wt.%, XRF; Table 1); Fe_2O_3 values were recalculated and expressed as FeO_t (see Methods).

3.3. Trace Elements and Rare Earth Elements (REE)

The trace element composition of Gamalama volcanic rocks reveals distinct geochemical patterns that provide insights into their magmatic history. Based on their behavior during magmatic processes, these elements can be categorized into compatible elements (Cr, Ni, Sc), which tend to partition into crystallizing minerals, and incompatible elements (K, Nb, Rb, Y, Th), which remain concentrated in the melt.

Our analyses show Sr (413–458 ppm) and Ba (215–315 ppm) as the most abundant trace elements. Other notable concentrations include Ga (19.1–22.1 ppm), Sc (18–25 ppm), Nb (2.1–2.7 ppm), and Cs (1.4–2.2 ppm), while Ta and Tb occur at concentrations below 1 ppm (Table 1).

To understand the tectonic setting of Gamalama volcano, we examined high field strength elements (HFSE), large-ion lithophile elements (LILE), and rare earth elements (REE) using established geochemical frameworks (Sun and McDonough, 1989; Senyah et al., 2016). The LILE group (Rb, Ba, Sr) shows considerable variation among samples, likely reflecting differences in magma differentiation history. The tendency of these elements to concentrate in residual melts with increasing SiO_2 content suggests significant plagioclase fractionation during magmatic evolution (James et al., 2021).

Chondrite-normalized REE patterns (Fig.10a; Nakamura, 1974; McDonough and Sun, 1995) reveal characteristic enrichment of light REE (LREE: La–Sm) relative to heavy REE (HREE: Gd–Lu). The La/Sm_n ratios of 3–4, coupled with Gd/Lu_n ratios of 10–12, indicate moderate LREE fractionation with relatively flat HREE trends-a signature typical of arc-related magmas. These patterns are consistent with partial melting of a mantle wedge, where LREE enrichment suggests relatively lower melting degrees, while the flat HREE trends may indicate limited garnet involvement in the source region (Meshesha et al., 2021).

Notably, the REE patterns show similarity to andesitic samples from West Halmahera (Ipranta and Irzon, 2019), supporting a shared subduction-related affinity across the region. The significant LREE enrichment, with La reaching 20–30 times chondritic values (Fig.10a), further confirms the calc-alkaline nature of Gamalama magmas (Rustioni et al., 2021). The weak negative Eu anomalies ($Eu/Eu^* = 0.28–0.33$) provide additional evidence for plagioclase fractionation during magma evolution (Lee et al., 2023).

Primitive mantle-normalized trace element patterns (McDonough and Sun, 1995; Fig.10b) display characteristic depletions in Ti and pronounced negative Nb–Ta anomalies. These HFSE depletions are considered diagnostic of subduction zone magmatism (Pearce and Peate, 1995), typically attributed to the retention of Nb and Ta in Ti-rich minerals within the subducting slab. This process results in slab-derived fluids that are enriched in LILE and LREE but depleted in HFSE (Brenan et al., 1994; Schmidt et al., 2004), ultimately imparting these distinctive geochemical signatures to arc magmas.

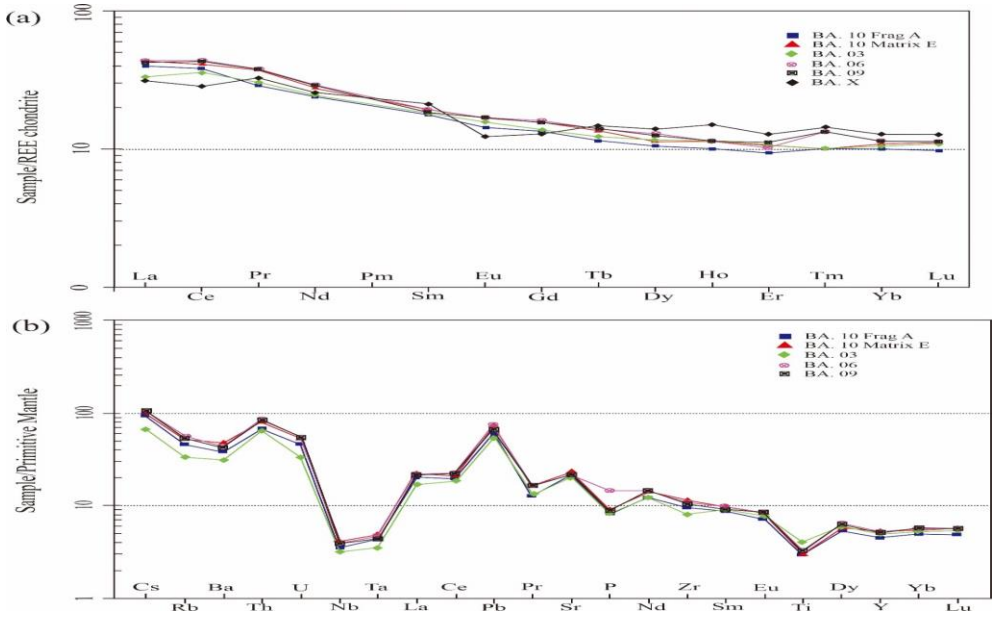


Fig.10. a) Chondrite-normalized rare earth element (REE) patterns for Gamalama volcanic rocks (normalization values after Nakamura, 1974). For comparison, an andesitic sample from West Halmahera (sample BA.X, Ipranta and Irzon, 2019); b) Primitive mantle-normalized trace element patterns (normalization values after McDonough and Sun, 1995)

4. Discussion

4.1. Magma Differentiation

Petrographic observations together with bulk-rock chemistry from Gamalama lavas allow us to reconstruct their evolutionary history. Classification plots-including the SiO_2–K_2O diagram (Peccerillo and Taylor, 1976) and AFM (Irvine and Baragar, 1971), are shown in Fig.11 and consistently place the rocks within the calc-alkaline field typical of convergent margins. This geochemical classification is supported by mineralogy: plagioclase (andesine–labradorite) dominates the phenocryst assemblage, with clinopyroxene and Fe–Ti oxides as common accessory phases. The absence of olivine further reinforces a calc-alkaline affinity.

Geochemical classification (TAS; Fig.7) and SiO_2–K_2O relations (Fig.10) place the samples in the medium-K, subalkaline basaltic–andesitic field, consistent with arc magmatism. AFM behavior (Fig.11) and Harker trends (Figs.8 and 9) indicate a calc-alkaline differentiation trajectory: FeO_t and MgO decline with increasing SiO_2 while alkalis (K_2O, Na_2O) and P_2O_5 rise. The negative CaO–SiO_2 trend, together with petrographic evidence, points to early clinopyroxene fractionation; concurrent TiO_2 and FeO_t declines imply early Fe–Ti oxide crystallization. Later-stage plagioclase growth is inferred from the positive Al_2O_3–SiO_2 relation and the prevalence of plagioclase phenocrysts. The relatively high Na_2O values are primarily attributed to magma differentiation and contributions from the groundmass, despite the absence of albite (Larsen et al., 2010; Santos and Hartmann, 2021).

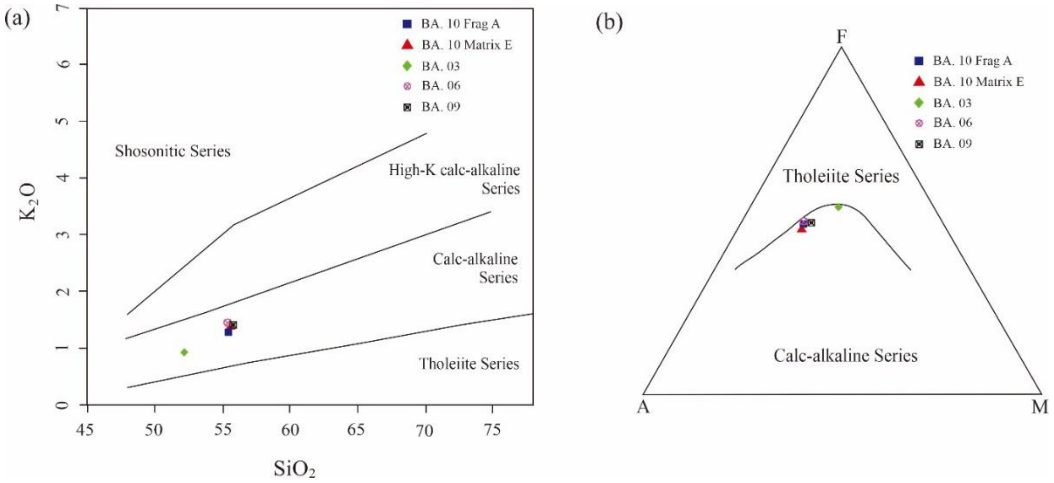


Fig.11. a) Distribution of igneous rock samples from Gamalama Volcano on the SiO_2–K_2O diagram (after Peccerillo and Taylor, 1976) showing samples plotting in the calc-alkaline field; b) AFM diagram (A = Na_2O + K_2O; F = FeO_t; M = MgO) after Irvine and Baragar (1971) showing a calc-alkaline differentiation trend. Whole-rock major-element data (wt.%, XRF; Table 1); Fe_2O_3 values were recalculated and plotted as FeO_t (see Methods)

Although fractional crystallization may be the dominant process, scatter in several oxide–SiO_2 plots (low *R* values; Fig. 9) could reflect the influence of intermittent open-system processes, such as periodic magma recharge or magma mingling, that are superimposed on the general fractional crystallization trend, although other factors cannot be excluded. Localized chloritization is consistent with limited hydrothermal overprint and may have contributed to local modification of Eu and other trace element distributions; therefore, subtle Eu anomalies are interpreted cautiously and require further validation.

Taken together, petrography and major-element systematics support a model in which a basaltic-andesitic parent magma evolved chiefly by clinopyroxene and Fe–Ti oxide fractionation, followed by late plagioclase crystallization, with episodic mixing producing the observed compositional scatter.

Trace-element and REE systematics below provide independent constraints on source characteristics, slab-derived inputs, and melting processes that complement the major-element interpretation.

4.2. Tectonic Setting

Trace-element and REE systematics (see Fig. 10) are consistent with a subduction zone origin for Gamalama magmatism. The chondrite-normalized REE patterns show LREE enrichment relative to HREE, and the primitive-mantle normalized multi-element plot highlights strong LILE enrichment coupled with pronounced negative Nb–Ta anomalies, which are commonly interpreted as diagnostic of arc magmatism in many studies (Nakamura, 1974; McDonough and Sun, 1995).

These features are consistent with subduction-zone processes. The enrichment of LREE despite low MgO (2.69 wt%), which is indicative of an evolved magma composition, suggests the influence of mafic mineral fractionation or assimilation–fractional crystallization (AFC) processes (Pearce and Peate, 1995). The negative Nb–Ta anomaly is most commonly attributed to either: (i) sequestration of Nb–Ta into rutile during dehydration/partial melting of eclogitic slab lithologies ("rutile control"); or (ii) fractionation and partitioning processes associated with highly saline, slab-derived fluids. Both mechanisms have been demonstrated experimentally to generate Nb–Ta depletion under realistic slab conditions. Thus, rutile control and saline-fluid transport are best regarded as viable, non-exclusive explanations for the Gamalama trace-element signature (Rustioni et al., 2019; Rustioni et al., 2021).

Case studies such as the Futuna Trough provide a stark reminder that a single sample or short stratigraphic section may capture only a transient state of the magmatic system. Such snapshots risk overlooking longer-term evolutionary trends in the mantle source (Haase et al., 2024). In addition to slab inputs, the ambient composition and depletion state of the mantle wedge will have strongly influenced the final magma chemistry. Variations in mantle-wedge composition and thermal structure can significantly modulate trace-element ratios and REE slopes. Accordingly, the Gamalama signature is best interpreted as the integrated product of slab-derived components interacting with a variably pre-conditioned mantle wedge.

Independent constraints are provided by tectonic discrimination diagrams. In the La/Yb vs. Th/Nb plot (Hollocher et al., 2012) (Fig.12a), all Gamalama samples plot within the volcanic arc field, consistent with contributions from the subducting slab to the mantle source. A similar arc affinity is supported by the La/Yb vs. Nb/La diagram (Hollocher et al., 2012; Fig.12b), where the lavas also cluster within the arc field. The consistency between these independent discrimination schemes reinforces the interpretation of a subduction zone setting.

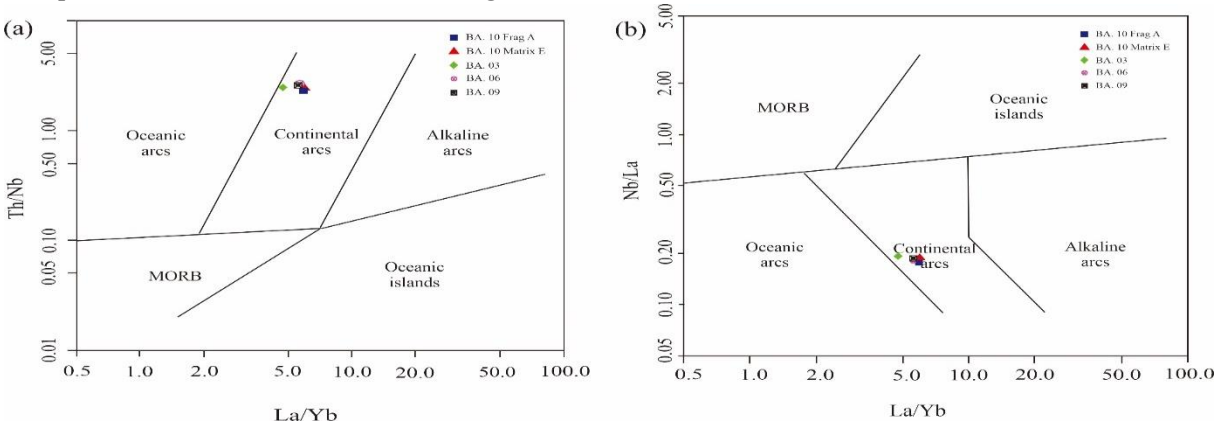


Fig.12. Tectonic discrimination diagrams for Gamalama volcanic rocks based on whole-rock trace-element data (ppm; Table 1): a) La/Yb vs Th/Nb; b) La/Yb vs Nb/La (after Hollocher et al., 2012). Both diagrams consistently place the samples in the volcanic-arc field, supporting a subduction-related origin.

Regionally, these features align with the geodynamic context of the Halmahera Arc, where eastward subduction of the Molucca Sea Plate sustains calc-alkaline volcanism with similar geochemical characteristics. The resemblance between Gamalama's trace-element patterns and those of andesites from West Halmahera suggests a shared subduction-related petrogenetic history across the arc, despite geographic separation.

Taken together, petrographic observations, trace-element systematics, and tectonic discrimination diagrams offer a consistent model for understanding magma genesis and evolution within an active convergent margin. We emphasize that the interpretations presented here are based on a limited dataset representing a single eruptive phase (Young Gamalama). While the combined petrographic and geochemical evidence provides a coherent framework for magma evolution, a comprehensive understanding will require integration with complementary approaches, including geochronology, volatile geochemistry, geophysical monitoring, and detailed stratigraphic analysis. Accordingly, this study is best regarded as a baseline framework for future multidisciplinary investigations aimed at fully characterizing Gamalama's magmatic system. Such integrated efforts will not only advance our understanding of arc magma systems in eastern Indonesia but also support hazard assessment and risk mitigation for Gamalama, one of the region's most active and densely populated volcanoes.

5. Conclusions

The Batu Angus lava of Gamalama Volcano is basaltic–andesitic and belongs to the calc-alkaline series typical of arc magmatism. Petrographic and geochemical data together indicate a magmatic evolution dominated by early clinopyroxene and Fe–Ti oxide fractionation, followed by late-stage plagioclase crystallization, with periodic magma mixing superimposed on this differentiation trend. Trace-element and REE patterns, including LILE enrichment and negative Nb–Ta anomalies, confirm a subduction-related arc affinity within the Halmahera Arc, consistent with eastward subduction of the Molucca Sea Plate. Minor alteration of plagioclase to chlorite reflects localized hydrothermal overprint but does not obscure the primary magmatic signature. Taken together, these results provide a coherent framework for magma genesis and evolution in the Young Gamalama system, while also emphasizing that broader temporal and spatial trends must be addressed through future multidisciplinary studies.

Acknowledgments

The authors are grateful to the Ministry of Research, Technology and Higher Education (RISTEKDIKTI) for funding this study in the scheme of Doctoral Dissertation Research with contract number 02035/UN4.22/PT.01.03/2024. The authors also gratefully acknowledge Faisal Saleh, M. Reza, Haliya, and Akbar Uta for their support in field data collection.

References

Ansori, C., Iriyanto, N., Hastria, D., Taniardi, P.N., Arif, A.K.D., 2024. Geoarchaeology, preliminary study of relationship analysis between geological conditions and the Megalithic sites in the candidate of Ternate Geopark, North Maluku. In: Proceeding international conference on geological engineering and geoscience, Yogyakarta, Indonesia, 1373(1), 012037. https://doi.org/10.1088/1755-1315/1373/1/012037

Awal, S., Kamur, S., Ajid, F., 2020. The Phenomenon of existence Batu Angus on the eastern slopes of mount Gamalama, Ternate Island, North Maluku. In: Proceeding international conference on Science Education and Technology, Indonesia, 1511(1), 012084. https://doi.org/10.1088/1742-6596/1511/1/012084

Bani, P., Nauret, F., Oppenheimer, C., Aiuppa, A., Saing, B.U., Haerani, N., Alfianti, H., Marlia, M., Tsanev, V., 2021. Heterogeneity of volatile sources along the Halmahera arc, Indonesia. Journal of Volcanology and Geothermal Research, 418(107342), 1–12. https://doi.org/10.1016/j.jvolgeores.2021.107342

Brenan, J. M., Shaw, H.F., Phinney, D.L., Ryerson, F.J., 1994. Rutile-aqueous fluid partitioning of Nb, Ta, Hf, Zr, U and Th: implications for high field strength element depletions in island-arc basalts. Earth and Planetary Science Letters, 128(3–4), 327–339. https://doi.org/10.1016/0012-821X(94)90154-6

Bronto, S., Hadisantono, R.D., Lockwood, J.P., 1982. Geological map of Gamalama Volcano, Ternate, North Maluku, scale 1: 25,000. Volcanological Survey of Indonesia. Bandung.

Chin, E.J., Shimizu, K., Bybee, G.M., Erdman, M. E., 2018. On the development of the calc-alkaline and tholeiitic magma series: A deep crustal cumulate perspective. Earth and Planetary Science Letters, 482, 277–287. https://doi.org/10.1016/j.epsl.2017.11.016

Deer, W.A., Howie, R.A., Zussman, J., 2013. An Introduction to the Rock-Forming Minerals, An Introduction to the Rock-Forming Minerals. https://doi.org/10.1180/dhz

Gill, R., 2010. Igneous Rocks and Processes: A Practical Guide (1st ed). Wiley-Blackwell, A John & Sons, Ltd., Publication, UK.

Global Volcanism Program, 2025. Gamalama (268060) in Volcanoes of the World (v. 5.3.1; 6 Aug 2025). Smithsonian Institution. Available at: https://volcano.si.edu/volcano.cfm?vn=268060 https://doi.org/10.5479/si.GVP.VOTW4-2013

Guo, X., Chen, N., 2025. Hornblende and Plagioclase Micro-Texture and Compositions: Evidence for Magma Mixing in High-Mg Adakitic Pluton, North China Craton. Minerals, 15(6), 1–30. https://doi.org/10.3390/min15060604

Haase, K. M., Regelous, M., Beier, C., Koppers, A.A.P., 2024. Slab steepening and rapid mantle wedge replacement during back-arc rifting in the New Hebrides. Nature Communications, 15(6070), 1–11. https://doi.10.1038/s41467-024-50445-3

Hall, R., Spakman, W., 2015. Mantle structure and tectonic history of SE Asia. Tectonophysics, 658, 14–45. https://doi.org/10.1016/j.tecto.2015.07.003

Harker, A., 1909. The natural history of igneous rocks. Cambridge University Press, London.

Hidayat, A., Marfai, M.A., Hadmoko, D.S., 2020. The 2015 eruption of Gamalama volcano (Ternate Island–Indonesia): precursor, crisis management, and community response. GeoJournal, 87(1), 1–20. https://doi.org/10.1007/s10708-020-10237-w

Hinschberger, F., Malod, J.A., Rehault, J.P., Villeneuve, M., Royer, J.Y., Burhanuddin, S., 2005. Late Cenozoic geodynamic evolution of eastern Indonesia. Tectonophysics, 404, 91–118. https://doi.org/10.1016/j.tecto.2005.05.005

Hollocher, K., Robinson, P., Walsh, E., Roberts, D., 2012. Geochemistry of amphibolite-facies volcanics and gabbros of the Støren Nappe in extensions west and southwest of Trondheim, Western Gneiss Region, Norway: a key to correlations and paleotectonic settings. American Journal of Science, 312(4), 357–416. https://doi.org/10.2475/04.2012.01

Ipranta, I., Irzon, R., 2019. Plagioclase fractionation on the Holocene volcanic rocks evolution in West Halmahera Regency. Jurnal Geologi dan Sumberdaya Mineral, 20(3), 165–174. https://doi.org/10.33332/jgsm.2019.v20.3.165-174p

Irvine, T.N., Baragar, W.R.A., 1971. A guide to the chemical classification of the common volcanic rocks. Canadian Journal of Earth Sciences, 8, 523–548. https://doi.org/10.1139/e71-055

James, E., Ghani, A.Z., Akinola, O.O., Asis, J., 2021. Petrology and geochemical features of Semporna Volcanic rocks, South-east Sabah, Malaysia. Sains Malaysiana, 50(1), 9–21. https://doi.org/10.17576/jsm-2021-5001-02

Korkmaz, G.G., Kurt, H., 2021. Interpretation of the Magma Chamber Processes with the help of Textural Stratigraphy of the Plagioclases (Konya-Central Anatolia). European Journal of Science and Technology, 25, 222–237. https://doi.org/10.31590/ejosat.898587

Kunrat, S., Bani, P., Haerani, N., Saing, U.B., Aiuppa, A., Syahbana, D.K., 2020. First gas and thermal measurements at the frequently erupting Gamalama volcano (Indonesia) reveal a hydrothermally dominated magmatic system. Journal of Volcanology and Geothermal Research, 407, 107096. https://doi.org/10.1016/j.jvolgeores.2020.107096

Larsen, J.F., Nye, C.J., Coombs, M.L., Tilman, M., Izbokev, P., Cameron, C., 2010. Petrology and geochemistry of the 2006 eruption of Augustine Volcano. In: Power, J.A., Coombs, M.L., Freymueller, J.T. (Ed.), The

2006 Eruption of Augustine Volcano. Alaska: U.S. Geological Survey Professional Paper 1769, 335–382. https://doi.org/10.3133/pp1769

Lee, S.G., Tanaka, T., Lee, M.J., 2023. Geochemical implication of Eu isotopic ratio in anorthosite: new evidence of Eu isotope fractionation during feldspar crystallization. Geosciences Journal, 27(3), 271–284. https://doi.org/10.1007/s12303-023-0009-6

Le Bas, M.J., Le Maitre, R.W., Streckeisen, A., Zanettin, B., IUGS Subcommission on the Systematics of Igneous Rocks., 1986. A chemical classification of volcanic rocks based on the total alkali-silica diagram. Journal of Petrology, 27(3), 745–750. https://doi.org/10.1093/petrology/27.3.745

McDonough, W.F., Sun, S.S., 1995. The composition of the Earth. Chemical Geology, 120, 223–253. https://doi.org/10.1016/0009-2541(94)00140-4

Meshesha, D., Chekol, T., Negussia, S., 2021. Major and trace element compositions of basaltic lavas from western margin of central main Ethiopian rift: enriched asthenosphere vs. mantle plume contribution. Heliyon, 7, e08634. https://doi.org/10.1016/j.heliyon.2021.e08634

Middlemost, E.A.K., 1994. Naming materials in the magma / igneous rock system. Earth-Science Reviews, 37(3–4), 215–224. https://doi.org/10.1016/0012-8252(94)90029-9

Molnár, K., Lahitte, P., Döncző, B., Arato, R., Szepesi. J., Benko, Z., Nomade, S., Gätjen, J., Dibacto. S., Temovski, M., 2023. Unravelling the pre-eruptive conditions of the rhyolitic Šumovit Greben lava dome from clinopyroxene-dominant glomeroporphyritic clots. Contributions to Mineralogy and Petrology, 178(83), 1–17. https://doi.org/10.1007/s00410-023-02066-0

Nakamura, N., 1974. Determination of REE, Ba, Fe, Mg, Na and K in carbonaceous and ordinary chondrites. Geochimica et Cosmochimica Acta, 38(5), 757–775. https://doi.org/10.1016/0016-7037(74)90149-5

Nesse, W.D., 1991. Introduction to Optical Mineralogy (2nd ed). Oxford University Press, New York.

Ningrum, R.W., Aryuni, V.T., Pambudi, N.A., 2019. Geothermal system characteristics on Northern Ternate region, Indonesia based on interpretation of magnetic anomalies. In: Proceedings of the 43rd Annual Scientific Meeting Himpunan Ahli Geofisika Indonesia, Semarang, Indonesia. https://doi.org/10.1088/1755-1315/367/1/012027

Nurahmah, S.C.C., Rosana, M.F., Haryanto, I., 2024. Karakteristik Petrografi dan Geokimia Unsur Utama Batuan Vulkanik Pulau Ponelo, Gorontalo Utara. Jurnal Geologi dan Sumberdaya Mineral, 25(4), 259–268. https://doi.org/10.33332/jgsm.geologi.v25i4.892

Olfindo, V.S.V., Payot, B.D., Valera, G.T.V, Jr. Gadot, E.G., Villaplaza, B.R.B., Tani, K., Dimalanta, C.B., Jr. Yumul, G.P., 2019. Petrographic and geochemical characterization of the crustal section of the Pujada Ophiolite, southeastern Mindanao, Philippines: Insights to the tectonic evolution of the northern Molucca Sea Collision Complex. Journal of Asian Earth Sciences, 184, 103994. https://doi.org/10.1016/j.jseaes.2019.103994

Pearce, J., Peate, D., 1995. Tectonic implications of the composition of volcanic arc magmas. Annual Review of Earth and Planetary Sciences, 23, 251–285. https://doi.org/10.1146/annurev.ea.23.050195.001343

Peccerillo, A., Taylor, S.R., 1976. Geochemistry of Eocene calc-alkaline volcanic rocks from the Kastamonu area, Northern Turkey. Contributions to mineralogy and petrology, 58(1), 63–81, https://doi.org/10.1007/BF00384745

Rezaei-Kahkhaei, M., Fransisco, C.G., Robert, Pankhurst, R.J., Esmaely, D., 2011. Magmatic differentiation in the calc-alkaline Khalkhab-Neshveh pluton, Central Iran. Journal of Asian Earth Sciences, 42(3), 499–514. https://doi.org/10.1016/j.jseaes.2011.04.022

Rustioni, G., Audétat, A., Keppler, H., 2019. Experimental evidence for fluid-induced melting in subduction zones. Geochemical Perspectives Letters, 11, 49–54. https//doi.org/10.7185/geochemlet.1925

Rustioni, G., Audetat, A., Keppler, H., 2021. The composition of subduction zone fluids and the origin of the trace element enrichment in arc magmas. Contributions to Mineralogy and Petrology, 176(51), 1–19. https://doi.org/10.1007/s00410-021-01810-8

Santos, J.O.S., Hartmann, L.A., 2021. Chemical classification of common volcanic rocks based on degree of silica saturation and CaO/K2O ratio. Anais da Academia Brasileira de Ciências, 93(3), 1–25. https://doi.org/10.1590/0001-3765202120201202

Scarani, A., Vona, A., Genova, D.D., Al-Mukadam, R., Romano. C., Deubener, J., 2022. Determination of cooling rates of glasses over four orders of magnitude. Contributions to Mineralogy and Petrology, 177(3), 1–17. https://doi.org/10.1007/s00410-022-01899-5

Schmidt, M. W., Dardon, A., Chazot, G., Vannucci, R., 2004. The dependence of Nb and Ta rutile-melt partitioning on melt composition and Nb/Ta fractionation during subduction processes. Earth and Planetary Science Letters, 226(3–4), 415–432. https://doi.org/10.1016/j.epsl.2004.08.010

Senyah, G.A., Dampare, S.B., Asiedu, D.K., 2016. Geochemistry and tectonic setting of the Paleoproterozoic metavolcanic rocks from the Chirano Gold District, Sefwi belt, Ghana. Journal of African Earth Sciences, (122), 32–46. https://doi.org/10.1016/j.jafrearsci.2015.07.022

Sheth, H.C., Torres-Alvarado, I.S., Verma, S.P., 2002. What is the "calc-alkaline rock series"?'. International Geology Review, 44(8), 686–701. https://doi.org/10.2747/0020-6814.44.8.686

Streckeisen, A., 1979. IUGS Subcommission on the Systematics of Igneous Rocks: Classification and nomenclature of volcanic. Geology, 7, 331–335. https://doi.org/10.1130/0091-7613(1979)7<331:CANOVR>2.0.CO;2

Suhardja, S.K., Ramdhan, M., Sulaiman, M.I., Pranata, B., Hidayat, E., Widiyantoro, S., Rawlinson, N., Anggono, T., Syuhada, Febriani, F., Dewi, C.N., Hasib, M., Jatnika, J., Prasetio, A.D., Setyonegoro, W., 2024. 3-D P-wave velocity structure of the upper mantle beneath eastern Indonesia from body wave tomography. Physics of the Earth and Planetary Interiors, 356, 107266. https://doi.org/10.1016/j.pepi.2024.107266.

Suhermat, M., Draniswari, W.A., Santoso, I., 2024. Remote Sensing of Gas Characteristics in 2018 Gamalama Eruption. In: Proceedings of the 5th International Conference on Geoscience and Earth Resources Engineering, Bandung. https://doi.10.1088/1755-1315/1437/1/012025

Sun, S.S., McDonough, W.F., 1989. Chemical and isotopic systematics of oceanic basalts: implications for mantle composition and processes. Geological Society, 42(1), 313–345. https://doi.org/10.1144/GSL.SP.1989.042.01.19

Tornos, F., Hanchar, J.M., Steele-MacInnis, M., Crespo, E., Kamenetsky, V.D., Casquet, C., 2024. Formation of magnetite-(apatite) systems by crystallizing ultrabasic iron-rich melts and slag separation. Mineralium Deposita, 59, 189–225. https://doi.org/10.1007/s00126-023-01203-w

Wang, D., Lin, F., Shi, M., Wang, H., Yang, X., 2023. Geological setting, tectonic evolution and spatio-temporal distributions of main mineral resources in South East Asia: A comprehensive review. Solid Earth Sciences, 8(1), 34–48. https://doi.org/10.1016/j.sesci.2022.12.003

Widiwijayanti, C., Tiberi, C., Deplus, C., Diament, M., Mikhailov, V., Louat, R C., 2004. Geodynamic evolution of the northern Molucca Sea area (Eastern Indonesia) constrained by 3-D gravity field inversion. Tectonophysics, 386, 203–222. https://doi.org/10.1016/j.tecto.2004.05.003

Yanny, Y., Ibrahim, M.M.Hi., Abbas, S.Hi, Muliadi, Jaya, A., Maulana, A., 2020. Geochemical composition and morphology study of Major Minerals of Angus Stone from Gamalama Mountain, Ternate Island, Indonesia. In: Proceedings international conference on science and technology 2019, Surabaya City, 1569(0420800), https://doi.org/10.1088/1742-6596/1569/4/042080

Zhao, S.W., Yang, C., Lai, S.C., Pei, X.Z., Li, Z.C., 2021. Multistage fractional crystallization in the continental arc magmatic system : constraints from the appinites in Tengchong Block, southeastern extension of Tibet. Lithosphere, 1–18.